Journal of Volcanology and Geothermal Research 178 (2008) 683–692

Contents lists available at ScienceDirect

Journal of Volcanology and Geothermal Research

journal homepage: www.elsevier.com/locate/jvolgeores

Emplacement conditions of igneous dikes in Ethiopian Traps

Richard A. Schultz [a,*], Daniel Mège [b], Hervé Diot [b,c]

[a] Geomechanics–Rock Fracture Group, Department of Geological Sciences and Engineering, University of Nevada, Reno, NV 89557 USA
[b] Laboratoire de Planétologie et Géodynamique, UMR CNRS 6112, Université de Nantes, 2 rue de la Houssinière, BP 92205, 44322 Nantes cedex 3, France
[c] Université de La Rochelle, Avenue Michel Crépeau, 17042 La Rochelle cedex 1, France

ARTICLE INFO

Article history:
Received 7 January 2008
Accepted 22 August 2008
Available online 11 September 2008

Keywords:
dikes
basalt
emplacement conditions
displacement–length scaling

ABSTRACT

The emplacement conditions for 39 igneous dikes cutting basalts in northwestern Ethiopia are evaluated by analyzing their displacement–length scaling relations. Maximum opening displacements and lengths of the dikes demonstrate displacement–length scaling of the form $D_{max}=0.088L^{0.48}$, consistent with other populations of dikes and veins and different than the power-law scaling relation typically found for faults. The dikes propagated through the thin Trap basalt sequence under conditions of constant fracture toughness, with values corrected for three-dimensional dike geometry of ~77–273 MPa $m^{1/2}$. The large values of fracture toughness are likely associated with (1) the toughening effects of near-tip damage, (2) mixed-mode dike propagation, as shown by magma flow fabric analysis through anisotropy of magnetic susceptibility (AMS) and image analysis of thin sections, and (3) elevated temperature within the blocky and ductile basaltic host rock, evidence of which has been found in the field.

1. Introduction

The emplacement conditions of igneous dikes can be evaluated by using the displacement–length (D–L) scaling relations of a dike set. In contrast to faults, which scale as $D_{max}=\gamma L^n$, with the exponent $n=1$ and therefore having a linear dependence of maximum displacement and discontinuity length (e.g., Cowie and Scholz, 1992; Clark and Cox, 1996; Schlische et al., 1996; Scholz, 1997, 2002; Schultz et al., 2006), veins and dikes scale as $n=0.5$ (in the power-law relation $D_{max}=\alpha L^{0.5}$), consistent with growth under conditions of constant rock properties (i.e. the host-rock fracture toughness, K_{Ic}) instead of constant driving stress (as in the case of faults) (e.g., Scholz, 2002, p. 116; Olson, 2003; Schultz et al., in press). Fracture toughness corresponds to the strength of the host rock in tension that resists dike propagation; as the internal magma pressure exceeds any dike-normal compressive stress, the dike dilates to a width determined by the host-rock stiffness, given by its Young's modulus and Poisson's ratio, eventually propagating when the stress intensity factor K_I at its tip equals the fracture toughness K_{Ic} (e.g. Pollard, 1987). Propagation ceases either when K_I decreases or K_{Ic} increases, or both (e.g. DeGraff and Aydin, 1993), making the factors that contribute to changes in K_I and K_{Ic} for dikes of primary importance to the understanding of dike emplacement and eruption conditions. We show in this paper how the displacement–length scaling relations for a set of dikes can provide quantitative values for the field-scale fracture toughness of the host rock at the time of dike emplacement, a key physical property that otherwise must be measured from small samples under laboratory conditions (e.g. Atkinson and Meredith, 1987; Balme et al., 2004).

Several previous studies have reported measurements of dike lengths and thicknesses including those of Gudmundsson (2002), Babiker and Gudmundsson (2004), Klausen (2006), and Ray et al. (2007). Although stress conditions associated with dike emplacement, such as excess magma pressure, have been estimated previously from dike measurements (e.g. Gudmundsson et al., 1999; Babiker and Gudmundsson, 2004; Gudmundsson, 2006), the properties of the host rock, such as its fracture toughness, were generally not evaluated from field measurements of dikes (but see Delaney and Pollard, 1981; Rubin and Pollard, 1987; Parfitt, 1991; Rubin, 1993).

In this paper we evaluate the emplacement conditions for a set of segmented igneous dikes in Ethiopia. The dikes are well expressed in satellite images and accessible in the field, permitting extraction of a high-quality dataset. The data demonstrate power-law D–L scaling with $n=0.48$, consistent with the few studies of segmented dikes and veins available in the literature (Olson, 2003; Schultz et al., in press). The resulting values of fracture toughness during dike emplacement are consistent with previous field-scale estimates, obtained by using independent techniques, for shale, granitic, and basaltic host rocks.

2. Ethiopian dike complex

The analyzed dike set is part of the 29–31 Ma NE–SW dike swarm identified by Mège and Korme (2004a) in the Ethio-Sudanese plain west of the Abyssinian volcanic plateau (the Trap Series), of similar

* Corresponding author.
E-mail addresses: schultz@mines.unr.edu (R.A. Schultz), daniel.mege@univ-nantes.fr (D. Mège), hdiot@univ-lr.fr (H. Diot).

0377-0273/$ – see front matter © 2008 Elsevier B.V. All rights reserved.
doi:10.1016/j.jvolgeores.2008.08.012

age (Fig. 1). This swarm, which contains hundreds of dikes, is the largest of the swarms that have been identified to date and is thought to have transmitted magma from the underlying Ethiopian mantle plume to the surface. The dikes are observed at the bottom level of the Trap Series, suggesting that they may have fed the lava flows over their total thickness. The dikes are surrounded by the

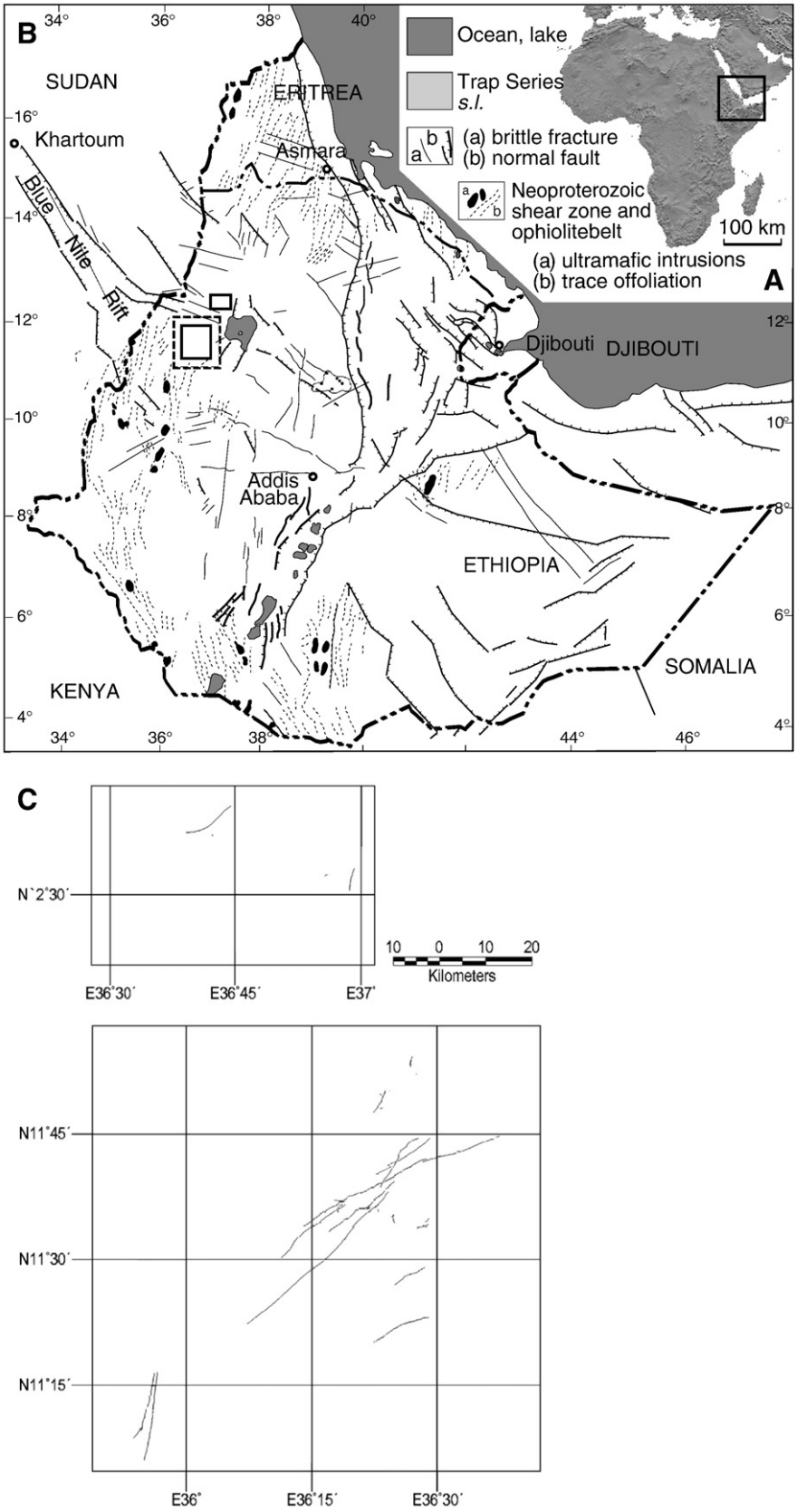

Fig. 1. A: Context map and location of B; B: brittle structure map of the African horn and location of C (black boxes) and the shaded relief map of Fig. 2 (black dashed box); C: location map of the 39 measured dikes.

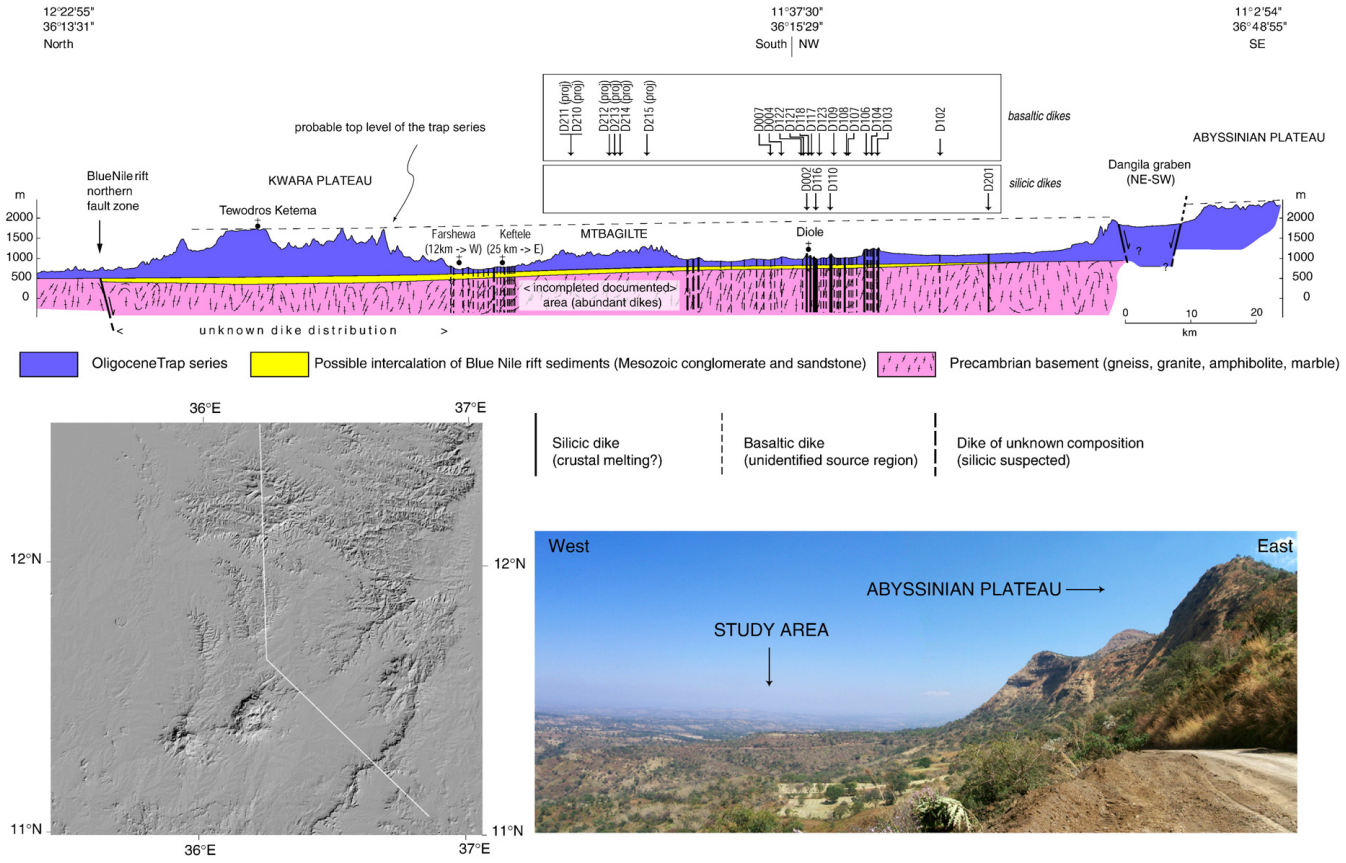

Fig. 2. Cross-section of the study area based on fieldwork. Topography from SRTM (Farr et al., 2007); geological interpretation from fieldwork, satellite imagery, and previous work including Seyid (2002), Mège and Korme (2004a, b), and Hautot et al. (2006). The studied dikes are located if they cross the profile or if their distance to the profile is less than a few km; dikes at a greater distance (up to 25 km) are also projected along the profile, in which case their ID is followed by "(proj)". The silicic dikes shown are true individual dikes; the basaltic dikes are too abundant to all be displayed here, so the figure gives an idea of their spatial distribution only. The location of nearby villages is given as indications for field access to the dikes.

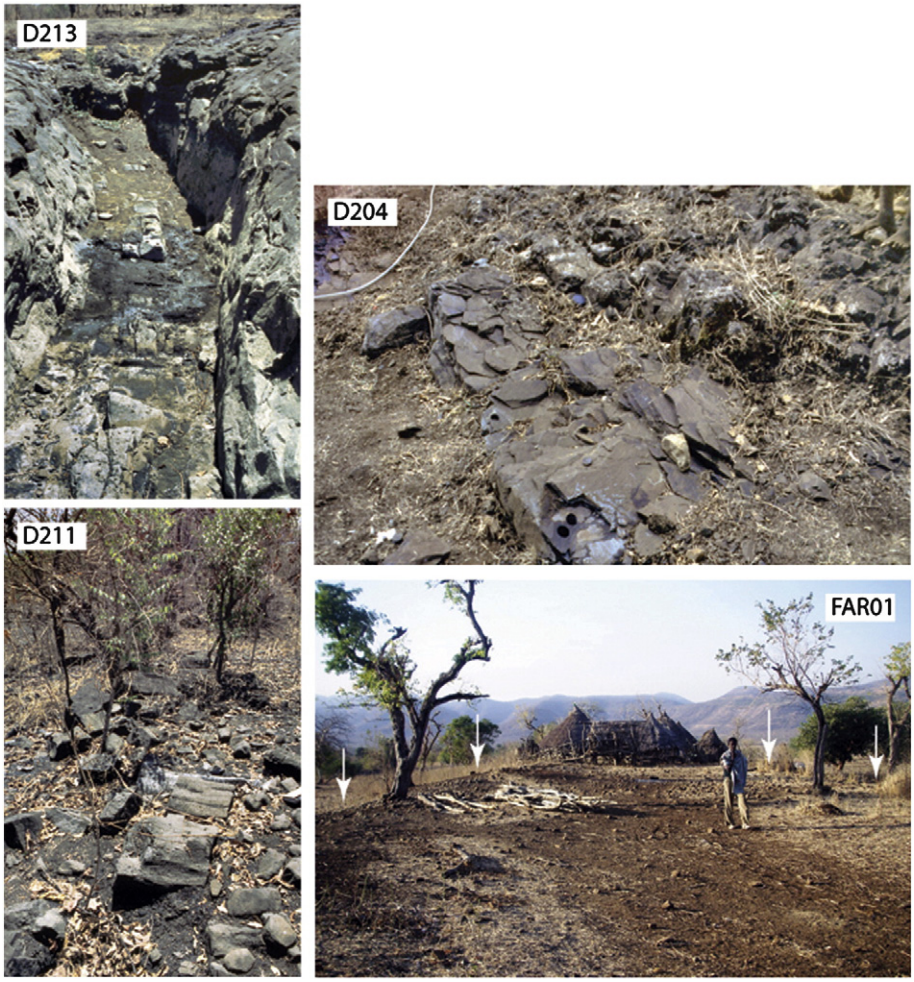

Fig. 3. Typical basaltic dike outcrops in the study area. The topography of dikes relative to the host rock of similar composition is probably governed to a large extent by the fracture density contrast. The topography of thin dikes is always less than 1 m either above or below the surrounding basaltic rock. For thicker dikes, the topography is usually higher than the surrounding rock by a few meters. D213: the thickness of many dikes can be measured in dry riverbeds. Note the dense fracture network within the dike parallel to its margins, which may explain its lower topography. D204, D211: in most cases, dike topography is not significantly different from the host rock, making field-based observation of chilled margins is essential for dike thickness determination. FAR01: typical thick basaltic dike (20 m) observed at Farshewa (see Fig. 2). Elevation above the surrounding rock is 1 to 2 m (the slope is indicated by arrows), which makes thickness measurements easy despite scarce chilled margins, whose observation requires excavation using a spear.

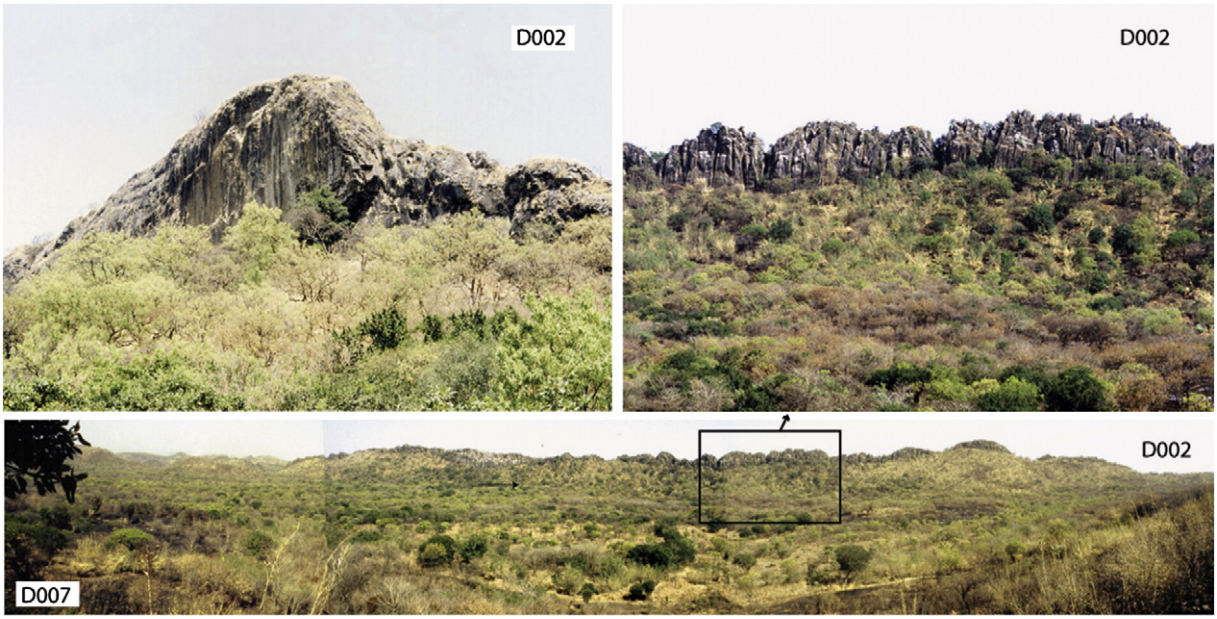

Fig. 4. Typical silicic dike outcrops (dike D002, the wide-angle view is taken from silicic dike D007). Silicic dikes can be easily measured both in the field and on satellite imagery owing to their dimensions and to the erosional contrast with the basaltic host rock in tropical environmental conditions. Dike D002 lies locally up to 60 m above the surrounding plain (top right). D002 segmentation is visible in the upper left of the wide-angle view; behind these segments, the farthest hills are segments of other silicic dikes.

Table 1
The studied dike population

Dike	Composition	Thickness (m)	Length (m)	Length error (+/−)	Latitude (Adindan)	Longitude
D002	Silicic	20	53,500	6500	N11°39′38.59″	E036°23′28.90″
D110	Silicic	13	25,150	14,850	N11°36′17.90″	E036°21′55.05″
D113	Silicic	4	17,600	600	N11°36′35.95″	E036°21′23.40″
D116	Silicic	5	16,000	3000	N11°36′06.64″	E036°17′40.36″
GBL02	Silicic	10	14,900	3	N11°11′25.65″	E035°55′58.66″
GBL03	Silicic	20	11,800	3	N11°10′57.28″	E035°54′56.72″
D201	Silicic	8.5	10,950	2950	N11°22′25.84″	E036°25′23.07″
DX	Silicic	10	1930	350	N12°37′42.88″	E036°40′21.49″
D007	Basaltic	7	19,000	3	N11°43′06.59″	E036°25′16.30″
D005	Basaltic	15	13,300	3	N11°41′51.99″	E036°24′42.00″
D102	Basaltic	7.5	7000	5000	N11°28′13.78″	E036°25′56.45″
D215	Basaltic	9	5350	2250	N11°48′37.21″	E036°22′35.35″
MTM03	Basaltic	5	4360	1160	N12°30′54.38″	E036°58′38.61″
D104	Basaltic	2.5	3940	910	N11°34′19.14″	E036°28′14.57″
D004	Basaltic	5	2700	3	N11°41′10.89″	E036°23′54.20″
D210	Basaltic	1.8	1990	1810	N11°53′37.81″	E036°26′21.54″
D120	Basaltic	1.2	1850	450	N11°37′12.33″	E036°18′11.85″
D107	Basaltic	2	1165	835	N11°35′29.46″	E036°24′29.73″
D001	Basaltic	2	1000	200	N11°35′03.99″	E036°28′38.70″
D122	Basaltic	1	1000	600	N11°37′11.91″	E036°18′04.27″
D111	Basaltic	1	895	315	N11°36′24.09″	E036°21′27.77″
D118	Basaltic	1	725	475	N11°36′33.49″	E036°17′53.59″
D108	Basaltic	2.5	600	100	N11°35′30.20″	E036°24′26.67″
D103	Basaltic	4	550	3	N11°34′15.05″	E036°28′28.01″
D214	Basaltic	1.2	520	3	N11°49′58.56″	E036°22′52.34″
MTM02	Basaltic	3.5	505	335	N12°32′30.10″	E036°55′43.65″
MTM04	Basaltic	2.7	460	130	N12°30′54.00″	E036°58′39.44″
D216	Basaltic	1	425	55	N11°48′18.60″	E036°22′52.83″
D117	Basaltic	1.5	400	100	N11°36′23.64″	E036°17′49.79″
D106	Basaltic	3.2	385	135	N11°34′23.55″	E036°28′08.50″
D115	Basaltic	2	385	85	N11°36′28.97″	E036°21′17.58″
MTM01	Basaltic	1.6	370	100	N12°37′11.51″	E036°42′07.69″
D123	Basaltic	2	330	90	N11°35′58.28″	E036°17′52.32″
D109	Basaltic	2	280	3	N11°36′11.77″	E036°22′39.30″
D114	Basaltic	1	270	80	N11°36′25.98″	E036°21′20.53″
D211	Basaltic	1.5	270	70	N11°53′37.81″	E036°26′21.54″
D212	Basaltic	0.6	230	3	N11°52′27.73″	E036°27′07.97″
D213	Basaltic	1	160	3	N11°50′27.67″	E036°23′55.85″
D112	Basaltic	0.6	60	3	N11°36′28.09″	E036°21′25.66″

main Abyssinian plateau to the east and by the Belaya and Kwara plateau remnants to the south and north. From the elevation difference between the study area and the surrounding plateau, a maximum paleodepth of emplacement is estimated to be 800–1000 m (Fig. 2). The dikes have been emplaced over a N–S to NE–SW-trending shear zone from the Tulu Dimtu Neoproterozoic orogenic belt (e.g., Allen and Tadesse, 2003). A thin eroded and discontinuous Mesozoic cover may exist within the NW–SE Mesozoic Blue Nile rift, which crosses the location of the later dike swarm (Mège and Korme, 2004a; Figs. 1 and 2). From correlation with sedimentary outcrops observed west of the study area, these sediments would be expected to be composed of conglomerate and sandstone whose age could not be resolved (Seyid, 2002). Magnetotelluric imaging has also revealed their probable existence east of the study area (Hautot et al., 2006).

The topography is almost flat, apart from the silicic dikes whose tops occasionally dominate the surrounding topography by tens of meters. The regional topography increases toward the Abyssinian plateau east of the study area, with a mean slope of 0.25°. Whether this slope corresponds to erosional processes or post-emplacement tilting is not known. The dikes show little evidence of post-emplacement rotation, although the dip angle of some dikes departs from 90° by ±10°, implying that they may have been tilted slightly after emplacement. If the regional topographic slope is not a direct consequence of regional tilting, the longest dikes may not be observed at a constant structural depth along strike. Small changes in depth of dike exposure would not, however, affect the measured values of dike thickness (equivalent to the dike opening displacement) significantly.

Fieldwork has revealed that most dikes are of basaltic composition (Fig. 3), but the longest (10–30 km) and thickest (5–20 m) are silicic (Fig. 4). Length distribution displays a typical cumulative length–frequency relation with a population exponent of −1.7 to −1.8 (Mège and Korme, 2004b), with no significant difference between the basaltic and silicic dikes.

Dike lengths were measured using Spot 2.5 m/pixel panchromatic imagery and multispectral imagery from ASTER (15 m/pixel) on which dikes are well emphasized by vegetation contrasts. Assessment of the *D*–*L* scaling relation on the ground is however limited by field access, which is necessary to obtain displacement data. In the Dangur, Alefa, and Metema districts of the Benishangul-Gumuz and Semien-Gonder administrative zones, 39 dikes, including 31 basaltic and 8 silicic, all segmented, could be followed for some distance in the field and their maximum thickness measured (Table 1). For the dikes thicker than 2 m, the field thickness data were also verified on Spot imagery. Maximum thickness (i.e., maximum displacement) was found to be

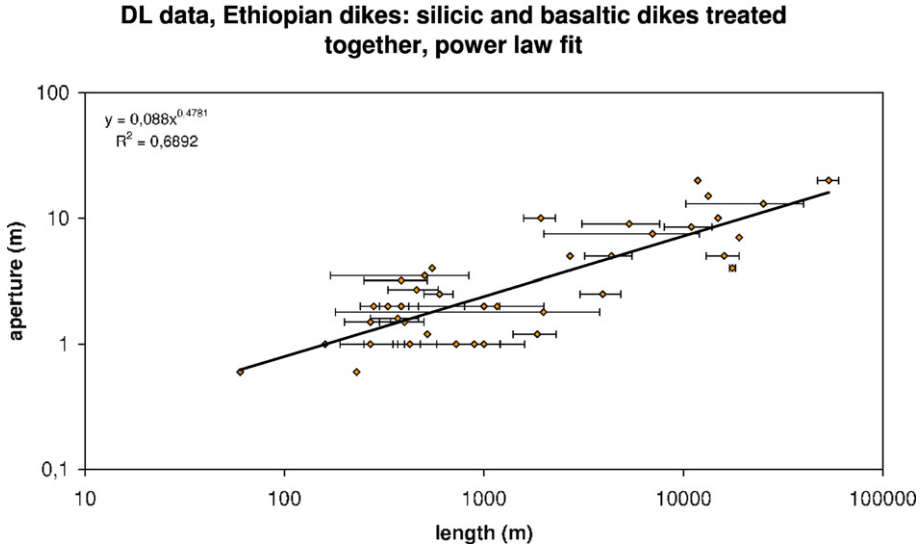

Fig. 5. Displacement–length relations for the 39 Ethiopian dikes. Error bars represent case-by-case uncertainty in length measurement on satellite imagery.

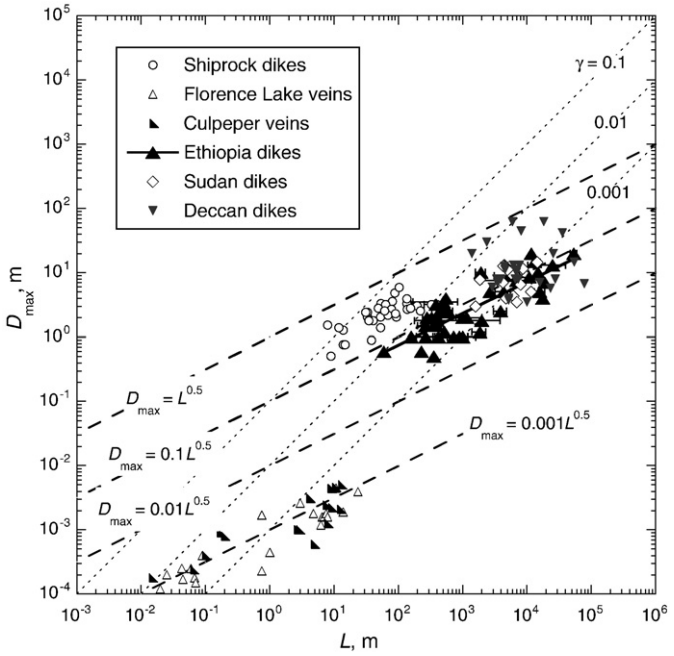

Fig. 6. Compilation of displacement–length relations for opening-mode fractures, after Schultz et al. (in press); data from Olson (2003), Babiker and Gudmundsson (2004), Ray et al. (2007), and this study. Lines of constant slope are shown: $n=1$, dotted, with $D/L=\gamma$; $n=0.5$, dashed.

0.5 m to 20 m, for lengths between 60 m and 53,500 m, and is usually close to the average thickness. The longest dike (D002, Serpent-God Dike, Mège and Korme, 2004a) has 29 main segments.

3. Results and discussion

The dike population (39 dikes) is described by the power-law relation $D_{max}=\alpha L^n$, with an exponent $n=0.48$ and a correlation coefficient $R^2=0.69$ (Fig. 5). We investigated the correlation and exponent for various dike subsets. The difference in lithology, i.e. in viscosity and propagation velocity for the basaltic and silicic dikes, does not appear to play a significant role in the scaling relation. The basaltic and silicic datasets, analyzed separately, give a poorer correlation and a lower exponent. $R^2=0.57$ and $n=0.47$ for the basaltic dikes $R^2=0.03$ and $n=0.11$ for the silicic dikes. The poor correlation and weak exponent for the silicic dikes may be explained by the small number of studied silicic dikes (8), and these numbers should not be considered to be significant.

Some dikes are observed to end close to the Abyssinian plateau. In order to investigate the possible issue that some of them may have segments that have not been exposed by plateau erosion yet, the basaltic dike population was capped at $L=10$ km. In this subpopulation, n decreases to 0.44 but R^2 decreases to 0.45. Conversely, in order to investigate the effect that dike length for short dikes is hard to ascertain both on satellite imagery and in the field due to their narrowness, a subpopulation in which the dikes shorter than 500 m were removed was investigated, giving $n=0.52$ and $R^2=0.6$. Whatever the dataset, the correlation is always higher using a power-law fit than a linear fit, and is better when the whole population rather than a fraction of it is used. Although meaningful, the correlation of the power law is never perfect, which may result from the fact that only segmented dikes having very strongly interacting or linked segments (large overlap and small spacing) are expected to closely follow a particular power-law relation (Olson, 2003).

The displacement–length data for the Ethiopian dikes are best described by $D_{max}=0.088\ L^{0.48}$ (Fig. 5), consistent with the scaling relations of other opening-mode fractures, including basaltic dikes intruding shales at Shiprock, New Mexico and two populations of veins (Fig. 6). The value of the power-law exponent, $n=0.48$, is consistent with a reduction in power-law exponent (or slope) for the dike array from the ideal value of $n=0.5$ appropriate to individual, isolated (noninteracting) dikes, following Olson's (2003) analysis for segmented fractures growing under $n=1.0$ conditions.

The displacement–length data from Ethiopia are consistent with those reported for dikes in Sudan by Babiker and Gudmundsson (2004) although the latter (open diamonds in Fig. 6) span a smaller length range (1.5–11.7 km) along with large scatter in the associated thickness measurements, inhibiting clear examination of their scaling relations. We infer that the fracture toughness of the granitic host rock investigated by Babiker and Gudmundsson (2004), however, is likely comparable to the basaltic host rock analyzed in this paper. The data reported by Ray et al. (2007) for dikes in the Deccan Traps of India (gray triangles in Fig. 6) of lengths 1.4–78.5 km have excessively large thickness variations attributed by Ray et al. (2007) to a combination of incomplete length determination (due to poor exposure of the dikes) and thermal erosion and associated widening of dike walls, neither effect of which is apparent in the Ethiopian dataset.

All four datasets are consistent with a power-law slope of about $n=0.5$, indicating propagation under conditions of constant rock fracture toughness, rather than constant driving stress, as in the case of faults (Scholz, 2002; Olson, 2003). These dike and vein populations can therefore be analyzed by assuming that they follow Linear Elastic Fracture Mechanics in the sense that their dimensions, scaling, and growth are regulated by the near-tip properties of the intruded rock; i.e. (Olson, 2003),

$$D_{max}=\frac{K_{Ic}(1-\nu^2)}{E}\frac{\sqrt{8}}{\sqrt{\pi}}\sqrt{L}=\alpha L^n \quad (1)$$

in which D_{max} is the maximum measured dike width, K_{Ic} is the host-rock fracture toughness, ν is Poisson's ratio, E is Young's modulus (all of the intruded host rock), and L is the horizontal length of the dike. Following Olson (2003, his Eq. (6)), this equation can be solved for fracture toughness by using the measured lengths L and maximum displacements D_{max} from a given dike population.

The Ethiopian dikes intruded a thin, <1 km-thick hydrothermally altered basaltic sequence that overlies Precambrian gneiss and amphibolite basement rocks with a possible thin intercalation of sediments. Following Schultz (1995), values of $E^*=5$–15 GPa and $\nu=0.3$

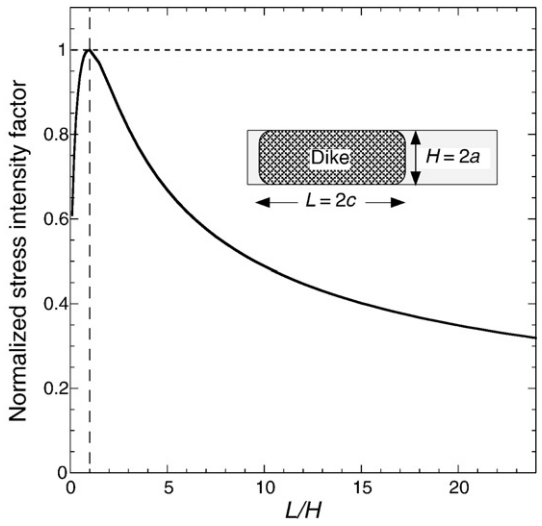

Fig. 7. Normalized stress intensity factor along the horizontal axis of a three-dimensional dike is plotted as a function of dike aspect ratio L/H. Inset shows dike geometry and parameters.

are used for the deformation modulus (i.e., field-scale Young's modulus (e.g., Schultz, 1996)) and Poisson's ratio, respectively, of the basaltic host rock, consistent with values of other basaltic sequences (Schultz, 1995; Gudmundsson, 2006) and those used by Rubin and Pollard (1987) in their study of dike propagation in Hawaiian basalts. Despite the possible presence of sediments, these modulus values represent lower bounds since the dike displacements may also reflect the stiffness of the basement as well as that of the thin sedimentary and basaltic carapace. A firm upper bound of E=70 GPa is estimated from values of Young's modulus for intact basalt or gneissic basement rocks (Turcotte and Schubert, 1982). Using these values gives K_{Ic}=584±326 MPa m$^{1/2}$ for the basalt sequence alone and 3876±2166 MPa m$^{1/2}$ for a basement-controlled sequence. Using values of Young's modulus of 70 GPa in Eq. (1), rather than deformation modulus, suggests that the field-scale values of basalt deformability (i.e., its deformation modulus, E^*) are more appropriate than values of Young's modulus E for intact rocks such as gneiss in a basement-controlled sequence.

Dike geometry (i.e. its horizontal length L and vertical or down-dip height H) influences the magnitude of the stress intensity factor K_I at its tip. The approach given in Eq. (1) assumes implicitly that the dikes are indefinitely tall, so that the vertical dike height $H \gg L$. However, the dike heights appear to have been limited by the thickness of the Trap Series basalts, which was probably less than about 1 km (Fig. 2, upper panel). The values of K_{Ic} calculated by using Eq. (1) (derived by equating the stress intensity factor K_I at the dike tip to the fracture toughness K_{Ic} of the host rock) must therefore be corrected for dike geometry given that their lengths (0.6–53 km) generally exceed their heights (H<1 km).

The stress intensity factor along the horizontal axis of a dike having length L=2c and height H=2a is given approximately by (Anderson, 1995, p. 59)

$$K_I = \sigma a \sqrt{\frac{\pi}{c\left[1 + 1.464\left(\frac{a}{c}\right)^{1.65}\right]}} \tag{2}$$

in which σ is the driving stress (i.e. excess magma pressure) acting to inflate the dike. K_{Ic} for a two-dimensional dike (i.e. having $H \gg L$) is given by $K_I = \sigma\sqrt{\pi c}$. The normalized stress intensity factor given by Eq. (2) divided by K_{Ic} for a two-dimensional dike is plotted as a function of dike aspect ratio L/H in Fig. 7. For aspect ratios L/H>1, typical of the Ethiopian dikes, the normalized stress intensity factor is less than one, with a value of ~0.3 for L/H=20. We infer that the value of K_{Ic} obtained from the dike scaling relations (Eq. (1)) should be reduced by perhaps a factor of 3 to account for the actual dike geometries; this leads to an estimate of fracture toughness for the host rock of approximately 77–273 MPa m$^{1/2}$.

Although the values estimated here for the basaltic host rock (assuming values of deformation modulus for the intruded basalts) exceed those of intact basalt by ~2 orders of magnitude (e.g., Atkinson and Meredith, 1987) they are consistent with other estimates for the fracture toughness of crustal rock. For example, values obtained by Olson (2003) for shale at the Shiprock dike swarm of 40–4000 MPa m$^{1/2}$ are comparable to, if somewhat greater than, estimates for the shale by Delaney and Pollard (1981) of 30–110 MPa m$^{1/2}$. Parfitt (1991) estimated K_{Ic} for Hawaiian basalt in the range of 30–110 MPa m$^{1/2}$. Theoretical estimates of fracture toughness exceeding 100 MPa m$^{1/2}$ were obtained by Rivalta and Dahm (2006) and Jin and Johnson (2008). The values of length and thickness reported by Babiker and Gudmundsson (2004) from dikes in Sudan, also plotted in Fig. 6, are consistent in their scaling with the Ethiopian dikes, implying a comparable value of fracture toughness for the intruded granites there.

Several factors may contribute to the large fracture toughness of the intruded basalts. First, the host rock is not intact basalt, but a jointed and altered basaltic rock mass. The tensile strength of the rock mass can be estimated by using

$$T_0 = \frac{K_{Ic}}{\sqrt{\pi c}} \tag{3}$$

in which K_{Ic} is the fracture toughness of the intact basalt blocks (taken to be ~2–3 MPa m$^{1/2}$; Balme et al., 2004) and c is interpreted as the appropriate grain or block size (e.g., Gudmundsson, 1992; Mandl, 2005, p. 17). Using values of K_{Ic}=2–3 MPa m$^{1/2}$ and c=5–30 cm in Eq. (3), the tensile strength of intruded basaltic rock mass is ~2–9 MPa, consistent with independent estimates of other basaltic rock masses

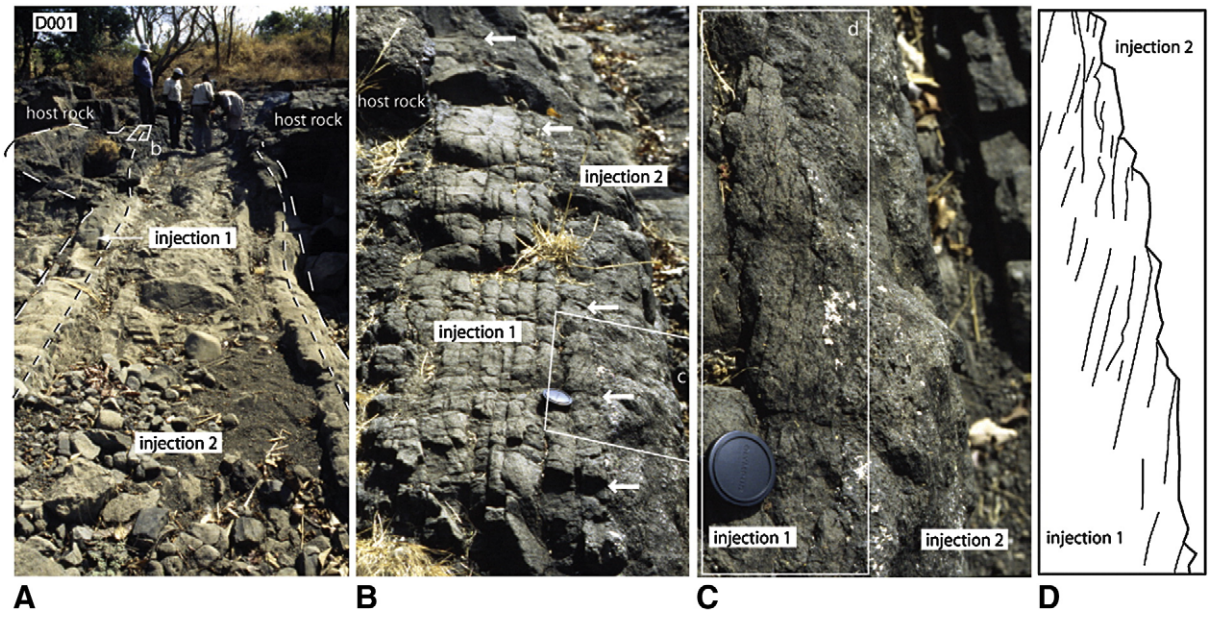

Fig. 8. (a) Detail of dike D001. Two injections are identified in the field: injection 1 is aphyric basalt, whereas injection 2 contains sanidine phenocrysts. Injection 1 displays echelon fractures (d, thin lines) abutting on the contact (d, thick line) with injection 2. The favored interpretation is localized jointing produced by injection 2, giving a left-lateral shear sense during dike emplacement. Dike thickness varies from 2 m (foreground) to 3 m (background), perhaps owing to local variations in modulus in still-hot host rock.

(e.g., Gudmundsson, 1992; Schultz, 1995). Such small values of tensile strength are likely to have been exceeded within a volume surrounding the tips of propagating igneous dikes (Rubin, 1993), due to elevated near-tip stress magnitudes there, thus increasing the intrinsic resistance to propagation of the dike in the rock mass. In structurally heterogeneous media encountered in materials science and

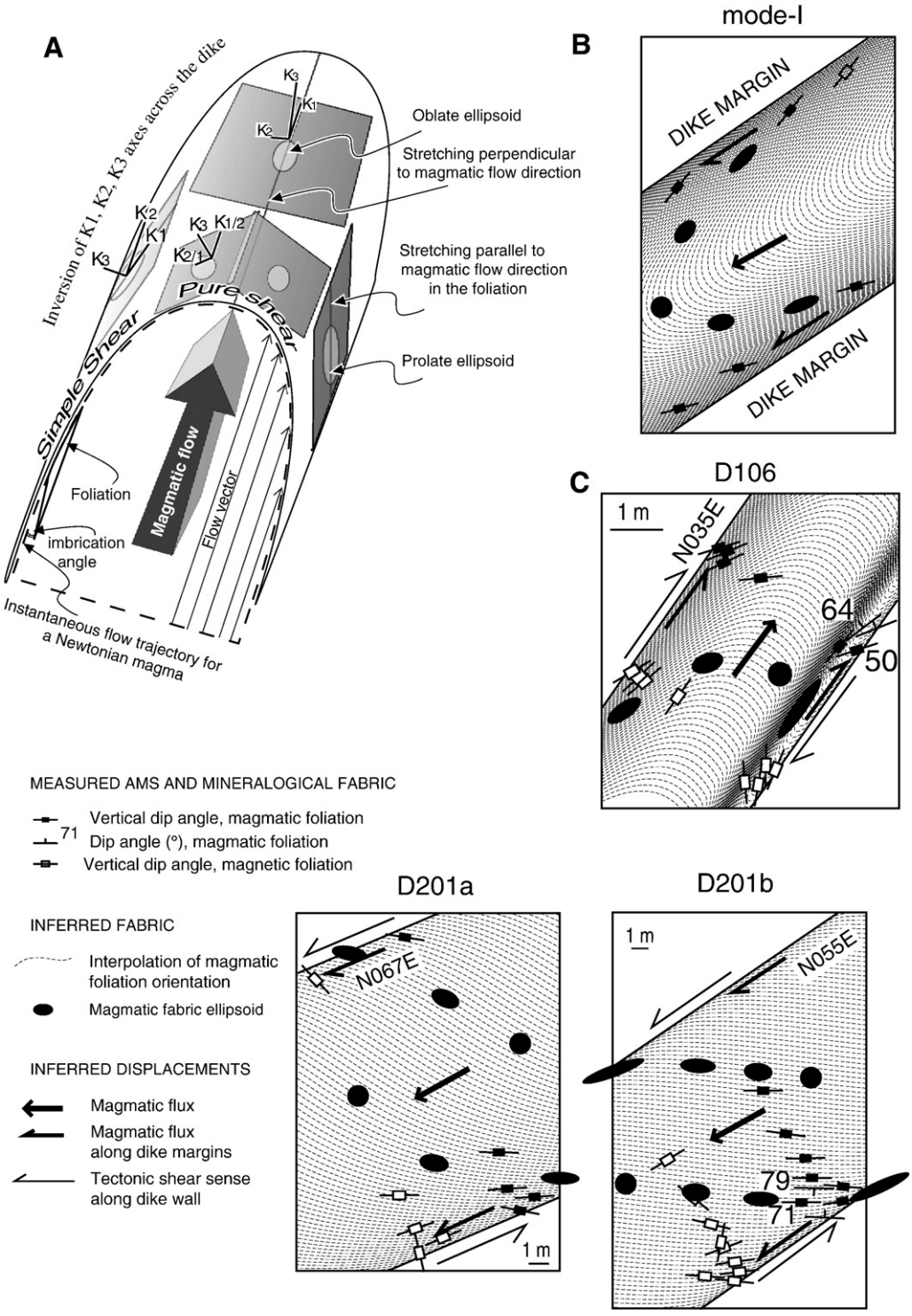

Fig. 9. Anisotropy of magnetic susceptibility (AMS) evidence of dike propagation oblique to the regional principal-stress orientations. (A) Magmatic and magnetic fabric evolution across a dike in the case where the dike margin is not sheared during emplacement, after Féménias et al. (2004). (B) Imbrication of magmatic and magnetic (K1–K2) foliation planes and fabric ellipsoid in map view in the absence of tectonic shearing and subhorizontal magma flow from the NE, comparable to the flow recorded in dike D201. In this case, lineations (not represented here) are everywhere subhorizontal with inclination <20° to the NE, and strike near the strike of the plane of illustration. (C) Imbrication of magmatic and/or magnetic (K1–K2) foliation planes along the margin of two Ethiopian dikes and interpretation. Dike D201a and D201b are two segments of D201. Foliation orientation indicators are located at their observed distance to the dike margins. The observed foliations (sample analysis given in Allaire, 2004) are not symmetrical and are therefore interpreted to result from syn-emplacement shearing at dike margins (Correa-Gomes et al., 2001; Féménias et al., 2004). Flux lines are interpolated from the orientation of the magmatic foliation, which is a reliable indicator of magma flow direction, in contrast to magnetic foliation which may be either parallel or orthogonal to the flow. For the two dikes there is no field evidence of internal chilled margins that would denote multiple injection events. Inversion of imbrication angles for dike D106 and dike segment D201a suggests that the velocity of tectonic displacement of the margins may have been higher than the magma velocity (Correa-Gomes et al., 2001).

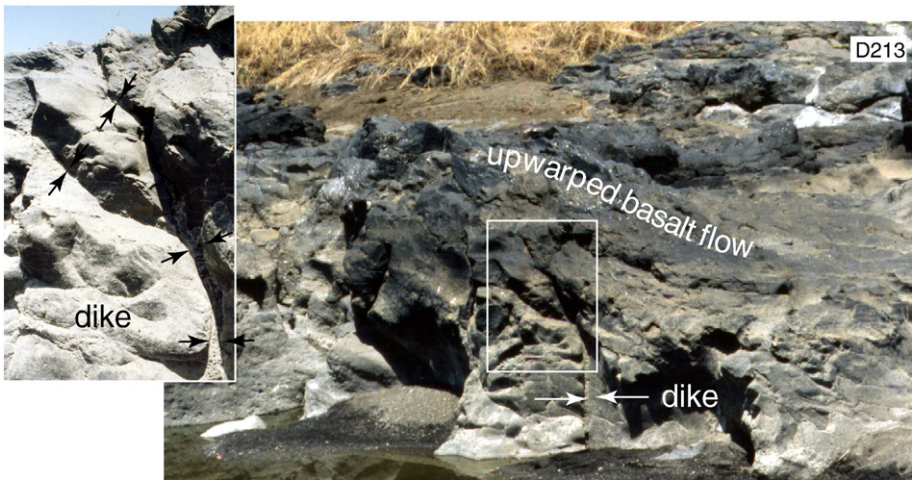

Fig. 10. Emplacement of dike D213 has displaced a pasty lava flow without cracking it, suggesting elevated temperature in the basaltic host rock. The dike, shown in Fig. 3 in a horizontal cross-sectional view in the bed of river Kwank, is shown here in vertical cross-section on the river bank at a distance of ~10 m from the location of Fig. 3.

engineering (e.g., Li and Liang, 1986), for example, an effective fracture toughness can be calculated that accounts for increased energy dissipation due to near-tip crack-related damage (Heald et al., 1972). For small ratios of (tensile) yield stress to driving stress suggested for basaltic dikes by Rubin (1993), the effective fracture toughness of basaltic rock mass probably is increased by a factor of at least 5–10. Damage-related toughening at length scales smaller than the cooling-column dimension similarly increases the resistance to crack propagation in Icelandic basaltic rock masses (Hatton et al., 1994).

Second, field observations (Mège and Korme, 2004a) indicate that the dikes intruded structurally anisotropic mylonitic and gneissic basement rocks within a Precambrian shear zone. Field evidence for syn- or post-emplacement shearing along several dike margins has been observed (Fig. 8). The geometric imbrication of the magmatic and magnetic foliations along dike margins implies syn-emplacement shearing as well (Fig. 9). Two basaltic dikes were sampled (one sampled along two distinct segments) that do not display macroscopic-scale evidence of shearing. The magmatic fabric was retrieved in the laboratory from image analysis of plagioclase laths which are the main-phase representative of the flow (Arbaret et al., 1996) and which were measured from three orthogonal thin sections (Allaire, 2004) cut on oriented samples using the intercept method (Launeau and Robin, 1996). This magmatic fabric is compared with that obtained from an anisotropy of magnetic susceptibility (AMS) analysis study (Launeau and Cruden, 1998). Magmatic and magnetic fabrics are usually in good agreement although the departure can be important, with the AMS measurements being more sensitive and representative of the subfabric of small crystals of magnetite and recording the last increment of magmatic flow. A high value of this departure is representative of rapid variation during the flow.

In principle, the magmatic foliation in case of pure mode-I dike opening (light gray dip symbols, Fig. 9B) presents symmetrical imbrications (Knight and Walker, 1988; Geoffroy et al., 2002), and the discrepancy between this geometry and the observed geometry is interpreted as the result of the combined influence of magma flux and wall-rock displacement before dike freezing (Correa-Gomes et al., 2001). Imbrication of magnetic foliation planes (K1–K2) commonly indicates magma flow orientation as well, but for reasons developed in Borradaile and Henry (1997) and Rochette et al. (1999), recently reinterpreted by Féménias et al. (2004), the principal magnetic axes may switch from the margin to the core of a dike even without margin shearing (Fig. 9A). For the two dikes sampled and investigated (Fig. 9C), the magmatic and magnetic fabrics argue in favor of syn-emplacement dike shearing, possibly with shearing along dike margins as well (dikes D201 and D106).

Macroscopic evidence and interpretation of magmatic and magnetic fabrics suggest that the orientations of the dikes were likely misaligned relative to the remote least compressive principal-stress direction (e.g., Ziv et al., 2000). In that case, propagation of the dikes would have been controlled by the mixed-mode fracture toughness of the rock mass, which is invariably larger than that associated with pure opening of a dike. On the other hand, propagation across the brittle structures of the Blue Nile rift, whose trend intersects those of the dikes at a high angle, rather than the low angle corresponding to the shear zone, should have negligibly affected fracture toughness.

Third, fracture toughness of basalt increases nonlinearly with temperature (DeGraff and Aydin, 1993; Balme et al., 2004), making dike propagation substantially more difficult for host-rock temperatures adjacent to the dike above ~150 °C than for host rock under ambient temperature (based on feldspar-rich Icelandic basalts tested by Balme et al., 2004, that may be most analogous mineralogically to the Ethiopian host basalt). Although the paleotemperature of the basaltic host rock during the time of dike emplacement is not known, similarity in the ages of the Trap Series basalts and the dikes (Mège and Korme, 2004a) suggests that temperatures of ~100–200 °C or more may be reasonable, contributing to perhaps a factor-of-two increase in the nominal fracture toughness and thereby an increased resistance to dike propagation. Fig. 10 shows the top of one of the studied dikes (D213) displacing a lava flow by non-cataclastic folding that must therefore have been pasty (i.e. ductile) during emplacement, supporting the inference of significantly elevated host-rock temperatures during dike emplacement. On Fig. 8a, the observed sudden increase of dike thickness within the same segment may also denote an associated decrease of the Young's modulus of the host rock (Eq. (1)) related to local variations of host-rock temperature.

4. Conclusions

Displacement–length measurements of igneous dikes in basalt from northwestern Ethiopia show a power-law scaling relation with an exponent ~0.5, indicating growth of the dikes under conditions of constant host-rock fracture toughness during their emplacement. The fracture toughness of the Trap Series basalts is estimated to be in the range of 77–273 MPa $m^{1/2}$, consistent with other estimates of the fracture toughness of crustal rocks intruded by igneous dikes. The values reflect the combined influences of three-dimensional dike geometry, low tensile strength, high temperature, and mixed-mode near-tip stresses, in the basaltic host rock during dike emplacement. Further work would further clarify the roles of paleotemperature, host-

rock mineralogy, near-tip damage, and oblique dilation on dike emplacement in this and similar areas where dike intrusion and shearing were coeval.

Acknowledgments

We thank Agust Gudmundsson and Stefano Santini for their detailed, constructive, and thoughtful reviews that improved the paper. This work was supported by NASA's Planetary Geology and Geophysics Program, CNRS/INSU Earth Observation Program, and CNES' ISIS program promoting scientific use of Spot satellite imagery.

References

Allen, A., Tadesse, G., 2003. Geological setting and tectonic subdivision of the Neproterozoic orogenic belt of Tuludimtu, western Ethiopia. J. Afr. Earth Sci. 36, 329–343.
Anderson, T.L., 1995. Fracture Mechanics: Fundamentals and Applications. CRC Press, Boca Raton, Florida.
Arbaret, L., Diot, H., Bouchez, J.L., 1996. Shape fabrics of particles in low concentration suspensions: 2D analogue experiments and application to tiling in magma. J. Struct. Geol. 18, 941–950.
Atkinson, B.K., Meredith, P.G., 1987. Experimental fracture mechanics data for rocks and minerals. In: Atkinson, B.K. (Ed.), Fracture Mechanics of Rock. Academic, London, pp. 477–525.
Allaire, R., 2004. Détermination du mode d'écoulement magmatique dans les dykes: analyse d'images et anisotropie de susceptibilité magnétique, application aux dykes d'Abyssinie, Ethiopie. M.Sc. thesis, Univ. La Rochelle, France.
Babiker, M., Gudmundsson, A., 2004. Geometry, structure and emplacement of mafic dykes in the Red Sea Hills, Sudan. J. Afr. Earth Sci. 38, 279–292.
Balme, M.R., Rocchi, V., Jones, C., Sammonds, P.R., Meredith, P.G., Boon, S., 2004. Fracture toughness measurements on igneous rocks using a high-pressure, high-temperature rock fracture mechanics cell. J. Volcanol. Geotherm. Res. 132, 159–172.
Borradaile, G.J., Henry, B., 1997. Tectonic applications of magnetic susceptibility and its anisotropy. Earth-Sci. Rev. 42, 49–93.
Cowie, P.A., Scholz, C.H., 1992. Physical explanation for the displacement–length relationship of faults using a post-yield fracture mechanics model. J. Struct. Geol. 14, 1133–1148.
Clark, R.M., Cox, S.J.D., 1996. A modern regression approach to determining fault displacement–length scaling relationships. J. Struct. Geol. 18, 147–152.
Correa-Gomes, L.C., Souza Filho, C.R., Martins, C.F.J.N., Oliveira, E.P., 2001. Development of symmetrical and asymmetrical fabric in sheet-like igneous bodies: the role of magma flow and wall-rock displacements in theoretical and natural cases. J. Struct. Geol. 23, 1415–1428.
DeGraff, J.M., Aydin, A., 1993. Effect of thermal regime on growth increment and spacing of contraction joints in basaltic lava. J. Geophys. Res. 98, 6411–6430.
Delaney, P.T., Pollard, D.D., 1981. Deformation of host rocks and flow of magma during growth of minette dikes and breccia-bearing intrusions near Ship Rock, New Mexico. U.S. Geol. Surv. Prof. Pap. 1202 61 pp.
Farr, T. G., et al., 2007. The shuttle radar topography mission. Rev. Geophys. 45, RG2004. doi:10.1029/2005RG000183.
Féménias, O., Diot, H., Berza, T., Gauffriau, A., Demaiffe, D., 2004. Asymmetrical to symmetrical magnetic fabric of dikes: paleo-flow orientations and paleo-stresses recorded on feeder-bodies from the Motru Dike Swarm (Romania). J. Struct. Geol. 26, 1401–1418.
Geoffroy, L., Callot, J.-P., Aubourg, C., Moreira, M., 2002. Magnetic and plagioclase linear fabric discrepancy in dykes: a new way to define the flow vector using magnetic foliation. Terra Nova 14, 183–190.
Gudmundsson, A., 1992. Formation and growth of normal faults at the divergent plate boundary in Iceland. Terra Nova 4, 464–471.
Gudmundsson, A., 2002. Emplacement and arrest of sheets and dykes in central volcanoes. J. Volcanol. Geotherm. Res. 116, 279–298.
Gudmundsson, A., 2006. How local stresses control magma-chamber ruptures, dyke injections, and eruptions in composite volcanoes. Earth-Sci. Rev. 79, 1–31.
Gudmundsson, A., Marinoni, L.B., Marti, J., 1999. Injection and arrest of dykes: implications for volcanic hazards. J. Volcanol. Geotherm. Res. 88, 1–13.
Hatton, C.G., Main, I.G., Meredith, P.G., 1994. Non-universal scaling of fracture length and opening displacement. Nature 367, 160–162.
Hautot, S., Whaler, K., Gebru, W., Desissa, M., 2006. The structure of a Mesozoic basin beneath the Lake Tana area, Ethiopia, revealed by magnetotelluric imaging. J. Afr. Earth Sci. 44, 331–338.
Heald, P.T., Spink, G.M., Worthington, P.J., 1972. Post yield fracture mechanics. Mater. Sci. Eng. 10, 129–138.
Jin, Z.-H., Johnson, S.E., 2008. Magma-driven multiple dike propagation and fracture toughness of crustal rocks. J. Geophys. Res. 113, B03206. doi:10.1029/2006JB004761.
Klausen, M.B., 2006. Similar dyke thickness variation across three volcanic rifts in the North Atlantic region: implications for intrusion mechanisms. Lithos 92, 137–153.
Knight, M.D., Walker, G.P.L., 1988. Magma flow directions in dikes of the Kooalu complex, Oahu, determined from magnetic fabric studies. J. Geophys. Res. 93, 4301–4319.
Launeau, P., Robin, P.-Y.F., 1996. Fabric analyses using the intercept method. Tectonophysics 267, 91–119.
Launeau, P., Cruden, A.R., 1998. Magmatic fabric acquisition mechanisms in a syenite: results of a combined anisotropy of magnetic susceptibility and image analysis study. J. Geophys. Res. 103, 5067–5089.
Li, V.C., Liang, E., 1986. Fracture processes in concrete and fiber reinforced cementitious composites. J. Eng. Mech. 112, 566–586.
Mandl, G., 2005. Rock Joints: the Mechanical Genesis. Springer, Berlin. 220 pp.
Mège, D., Korme, T., 2004a. Dyke swarm emplacement in the Ethiopian large igneous province: not only a matter of stress. J. Volcanol. Geotherm. Res. 132, 283–310.
Mège, D., Korme, T., 2004b. Fissure eruption of flood basalts from statistical analysis of dyke fracture length. J. Volcanol. Geotherm. Res. 131, 77–92.
Olson, J.E., 2003. Sublinear scaling of fracture aperture versus length: an exception or the rule? J. Geophys. Res. 108, 2413. doi:10.1029/2001JB000419.
Parfitt, E.A., 1991. The role of rift zone storage in controlling the site and timing of eruptions at Kilauea Volcano, Hawaii. J. Geophys. Res. 96, 10,101–10,112.
Pollard, D.D., 1987. Elementary fracture mechanics applied to the structural interpretation of dykes. In: Halls, H.C., Fahrig, W.F. (Eds.), Mafic Dyke Swarms. Geol. Assoc. Canada Spec. Pap., vol. 34, pp. 5–24.
Ray, R., Sheth, H.C., Mallik, J., 2007. Structure and emplacement of the Nandurbar–Dhule mafic dyke swarm, Deccan Traps, and the tectonomagmatic evolution of flood basalts. Bull. Volcanol. 69, 537–551.
Rivalta, E., Dahm, T., 2006. Acceleration of buoyancy-driven fractures and magmatic dikes beneath the free surface. Geophys. J. Int. 166, 1424–1439.
Rochette, P., Aubourg, C., Perrin, M., 1999. Is this magnetic fabric normal? A review and case studies in volcanic formations. Tectonophysics 307, 219–234.
Rubin, A.M., 1993. Tensile fracture of rock at high confining pressure: implications for dike propagation. J. Geophys. Res. 98, 15,919–15,935.
Rubin, A.M., Pollard, D.D., 1987. Origins of blade-like dikes in volcanic rift zones. In: Decker, R.W., Wright, T.L., Stauffer, P.H. (Eds.), Volcanism in Hawaii. U.S. Geol. Surv. Prof. Pap., vol. 1350, pp. 1449–1470.
Schlische, R.W., Young, S.S., Ackermann, R.V., Gupta, A., 1996. Geometry and scaling relations of a population of very small rift related normal faults. Geology 24, 683–686.
Scholz, C.H., 1997. Earthquake and fault populations and the calculation of brittle strain. Geowissenschaften 15, 124–130.
Scholz, C.H., 2002. The Mechanics of Earthquakes and Faulting, (2nd. ed.). Cambridge University Press. 471 pp.
Schultz, R.A., 1995. Limits on strength and deformation properties of jointed basaltic rock masses. Rock Mech. Rock Eng. 28, 1–15.
Schultz, R.A., 1996. Relative scale and the strength and deformability of rock masses. J. Struct. Geol. 18, 1139–1149.
Schultz, R.A., Okubo, C.H., Wilkins, S.J., 2006. Displacement–length scaling relations for faults on the terrestrial planets. J. Struct. Geol. 28, 2182–2193.
Schultz, R.A., Soliva, R., Fossen, H., Okubo, C.H., Reeves, D.M., in press. Dependence of displacement–length scaling relations for fractures and deformation bands on the volumetric changes across them. J. Struct. Geol. 30.
Seyid, G., 2002. Geology of the Abu Ramla Area (Includes Geological Map at the Scale of 1:250,000). Memoir 17, publ. #821-351-53. Geol. Survey Ethiopia, Addis Ababa. 133 pp.
Turcotte, D.L., Schubert, G., 1982. Geodynamics: Application of Continuum Physics to Geological Problems. Wiley, New York. 450 pp.
Ziv, A., Rubin, A.M., Agnon, A., 2000. Stability of dike intrusion along preexisting fractures. J. Geophys. Res. 105, 5947–5961.